Organic Materials and Organic/Inorganic Heterostructures in Atom Probe Tomography

Derk Joester,[1] * Andrew Hillier,[2] Yi Zhang,[2] and Ty J. Prosa[3]
[1] Materials Science and Engineering, Northwestern University, Evanston, IL 60208
[2] Chemical and Biological Engineering, Iowa State University, Ames, IA 50011
[3] Cameca Instruments Inc., 5500 Nobel Drive, Madison, WI 53711
* d-joester@northwestern.edu

Introduction

Nano-scale organic/inorganic interfaces are key to a wide range of materials. In many biominerals, for instance bone or teeth, outstanding fracture toughness and wear resistance can be attributed to buried organic/inorganic interfaces. Organic/inorganic interfaces at very small length scales are becoming increasingly important also in nano and electronic materials. For example, functionalized inorganic nanomaterials have great potential in biomedicine or sensing applications. Thin organic films are used to increase the conductivity of $LiFePO_4$ electrodes in lithium ion batteries, and solid electrode interphases (SEI) form by uncontrolled electrolyte decomposition [1]. Organics play a key role in dye-sensitized solar cells, organic photovoltaics, and nano-dielectrics for organic field-effect transistors. The interface between oxide semiconductors and polymer substrates is critical in emergent applications, for example, flexible displays [2].

Quantitative analysis of such interfaces is integral to controlling processing parameters, structure, and performance of the final device. However, the nanoscopic scale and chemical complexity of organic/inorganic interfaces makes imaging a challenge. Despite tremendous achievements in energy-filtered EM techniques [3], the development of synchrotron X-ray micro- and nano-probes [4], and the spectacular chemical detail of nano-SIMS [5], there is currently no technique that combines sub-nanometer resolution with chemical sensitivity across the *entire* periodic table. For example, even advanced electron microscopy (for example, STEM-EELS) is not suitable for detection of small quantities of some of the low-*Z* elements typical of biological materials or for determining lithium gradients and organic electrolyte breakdown products at the surface of lithium ion battery electrodes. There is mounting evidence, however, that laser-pulsed atom probe tomography (APT) will rise to the challenge. In the following, we discuss the pioneering early work and some exciting applications of APT to organic materials and organic/inorganic heterostructures made possible by the advent of UV laser pulsing in the atom probe.

Early Work

The ability to image organic molecules, in particular biomolecules, with atomic resolution has been a fascinating target since the early days of field electron emission microscopy (FEEM) and field ion microscopy (FIM). The work of the pioneers, E. Müller in the 1950s and J.A. Panitz in the 1980s, has been reviewed recently [6]. The first atom probe time-of-flight (TOF) spectra of conducting polypyrroles were reported by Nishikawa and Kato [7] and Maruyama and coworkers [8]. Nishikawa further reported on the TOF spectra of carbon allotropes, polythiophene, amino acids, and ionic liquids [9, 10]. Although these results represent a milestone in terms of chemical analysis, the great potential of APT in combining atomic-scale chemical and spatial information was not yet realized.

With the advent of pulsed-laser APT, it appears that the game is changing. The primary advantages of the pulsed-laser method are the near removal of all specimen electrical conductivity requirements and improved likelihood for successful analysis [6]. Laser pulsing heats the specimen tip surface, lowering the required electric field for field evaporation and, consequently, reducing premature specimen failure from stresses generated by the electric field. We discuss here the rapidly improving analysis capabilities for self-assembled monolayers [11–13], polymers [14–16], and the complex architecture of a tooth biomineral nanocomposite [17].

Methods and Materials

Sample preparation has a large influence on the performance of specimens during atom probe experiments. To arrive at a radius of curvature smaller than 20 nm, two basic strategies are used. Metallic samples (for example, Au, W) are commonly electropolished. Inorganic species, small molecules, and polymers can then be absorbed from solution, applied via dip coating, or by electrospray methods (here: P3HT polymer). In a variant of this technique, the electropolished needle is first conditioned by running it in the atom probe, effectively creating a shape that is ideal for atom probe and cleaning it of any contaminants. The analyte is then applied by adsorption from solution (here: bromide and hexanethiol monolayers). Samples that cannot be electropolished are usually fashioned into sharp tips by FIB-liftout and annular milling (here: organic thin-film sandwich structures, chiton tooth composite) [18].

An important aspect of sample preparation of organic samples is to prevent adsorption of organic species from the atmosphere. For example, Gordon and Joester carried out the entire following procedure in a nitrogen-filled oxygen- and water-free glove box [17]. Silicon wafers were coated with a 28 nm layer of Cr at a base pressure below 10^{-5} Pa (MBraun thermal evaporator, Garching Germany). A quartz crystal monitor was used to control film thickness (Inficon, East Syracuse, NY). The thermal evaporator was vented with dry nitrogen and the coated substrates were transferred within the glove box to a spin coater (Specialty Coating Systems G3P-B, Indianapolis, IN), where they were coated with a solution of chitin in hexafluoroisoproponol (1 mg·mL^{-1}) at 3000 rpm. The spin-coated substrates then coated with 200 nm of Ag at a base pressure below 10^{-5} Pa. The wafer was secured to an aluminum stub with a conductive adhesive carbon tab. The sample was then transferred through the atmosphere to the FIB/SEM, where specimen tips were prepared by lift-out and annular milling.

Results

Inorganic monolayers at surfaces. Self-assembled monolayers on metal surfaces are of interest not only in the context of electrochemical interfaces, but also as coatings, as model

systems for biological membranes, and as support for other analytes. Monolayers of bromide adsorbed on pre-sharpened gold tips were used as a simple test case. The mass spectral data show clear evidence of Au (Au^{n+}, n = 1–3), $AuBr^+$, and Br^+ with typical isotopic abundances (Figures 1A and 1B). In three-dimensional reconstructions, a dense bromide layer appears on the gold surface (Figure 1C). The thickness of this bromide layer is on the order of ~1 nm. The variation in coverage is presumably related to the nature of the underlying gold layer. However, the overall surface density of the bromide layer is ~1.5 ions nm^{-2}, which is within the same order as that observed with other surface techniques. This result demonstrates that APT can resolve a single, atomic layer of an adsorbed species, which suggests sufficient resolution for a variety of other thin-film systems.

Organic thin films: a self-assembled monolayer (SAM). Alkanethiolate monolayers are a well-studied class of monomolecular coatings that self-assemble into well-defined robust organic films on the surface of various metals. We examined a 1-hexanethiol (HT = $CH_3(CH_2)_4CH_2SH$) SAM formed on a pre-sharpened gold tip as a representative organic coating. Atom probe mass spectra show peaks associated with the organic SAM layer, for example, S^+, CH_3^+, and larger chain fragments (Figure 2). Even fragments corresponding to evaporation of entire molecules ($C_6H_{14-x}S^+$, x = 0–4) are observed. Interestingly, gold atoms appear not only as Au^+, but also in molecular ions as AuS^+, Au-SH^+, and $AuS(CH_2)_5CH_3^+$. The overall stoichiometry of the HT SAM determined by APT is $C_6H_{13.4}S$, in close agreement with the actual molecular composition $C_6H_{15}S$.

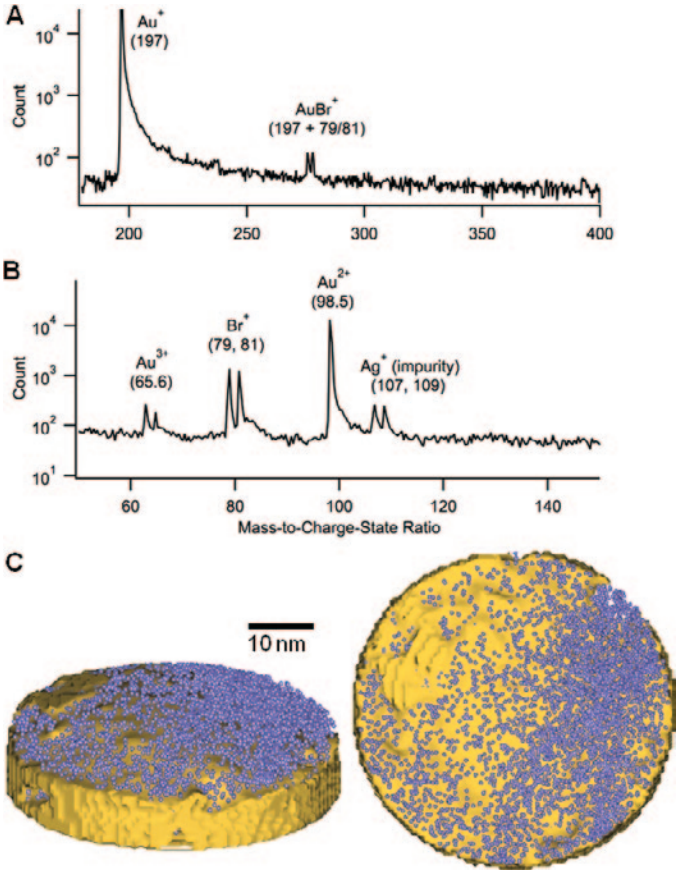

Figure 1: APT of bromide monolayer on gold tip. Mass spectrum of sample showing (A) Au^+ and $AuBr^+$ peaks in the high-mass region and (B) Au^{2+}, Au^{3+} and Br^+ in a lower mass range. (C) Three-dimensional reconstructions of bromide ions (spheres) on an isometric projection of the gold surface (left) and in plan view (right). Adapted with permission from Y Zhang and AC Hillier, *Anal Chem* 82 (2010) 6139–47. Copyright 2010 American Chemical Society.

In reconstructions, the hexanethiolate layer is located entirely on the surface of the gold tip (Figure 2 inset). Depth profiling indicates a relatively uniform carbon concentration through the layer until a depth of ~1.8 nm below the surface, where the C, H, and S concentrations decrease dramatically while the Au concentration increases to >95 at.%. This indicates a transition from the surface film to the bulk gold layer. While the overall geometry of the reconstruction is close to expectations, absolute values for thickness are overestimated substantially, by a factor of 2–4. This is likely due to artifacts of the reconstruction algorithm that does not yet account for the different properties of organic matter during field evaporation.

Polymers. The analysis and control over interfaces in flexible electronics or organic photovoltaic devices is critical for rational design and optimization. For example, composite films comprised of P3AT and PCBM are popular bulk heterojunction materials for organic photovoltaic devices. Compared to inorganic materials and organic thin films, atom probe spectra of soft polymeric materials can be much richer in terms of the number of fragments observed. For example, when P3HT was deposited on pre-sharpened tips by dipping or electrospray, many different molecular ions differing by as little as $\Delta m/z$ = 1 were detected (Figure 3A) [14]. Many of these correspond to a series of molecular ions with the general formula $[C_nH_{2n\pm m}]^+$, where n = 1–6 and m is variable. For P3HT films doped with fullerene, entire C_{60}^{n+} ions and several large fragments (C_{12}^+, C_{18}^+) were observed (see Figure 3A inset).

Such rich spectra contain a lot of useful chemical information. However, evaporation of large molecular ions can be problematic for reconstructions as information about the structure and orientation of the molecular ion is lost, effectively reducing the spatial resolution. We discovered that sample preparation could help mitigate this problem. When a P3AT/PCBM mixture—chemically very similar to the C_{60}-doped P3HT—was sandwiched between a Si wafer and a sputtered aluminum contact, mass spectra collected from specimens that were lifted out using FIB were starkly different (Figure 3B). Atomic carbon (C^+, C^{2+}) is the dominant monatomic ion, and even moderate atomic-mass ions are completely absent from the mass spectrum. This encouraging observation highlights that there remains much to learn about the interplay between sample composition, specimen preparation,

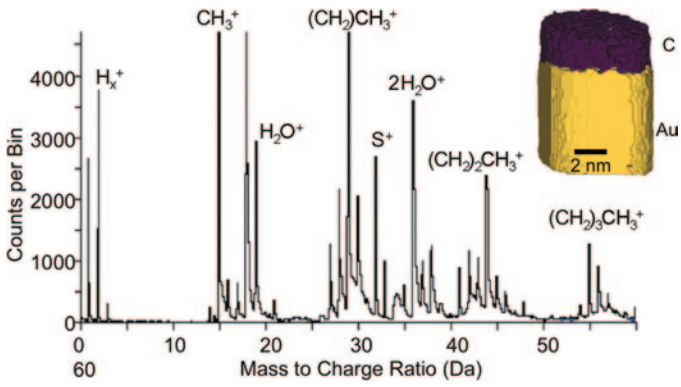

Figure 2: Mass spectrum of a monolayer of chemisorbed hexanethiol ($C_6H_{13}SH$) on gold. (inset) Isoconcentration surfaces for carbon and gold resulting from reconstruction of atom probe tomography data for the hexanethiol layer.

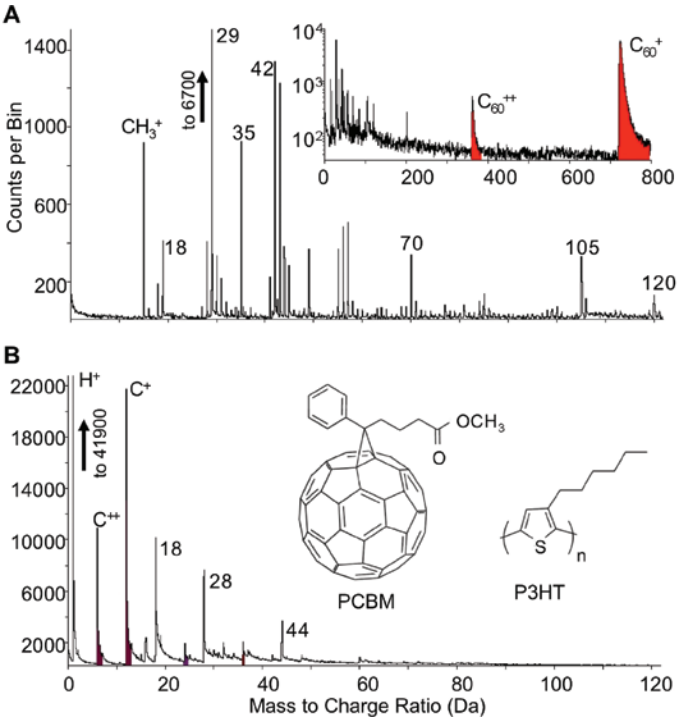

Figure 3: Atom probe tomography of C_{60}-doped P3HT polymer samples prepared by dipping (see A) or electrospray deposition on metal needle and FIB-lift-out (see B) of C_{60}-doped P3HT thin film sandwiched between Si wafer and sputtered Al. (A) Typical mass spectrum showing characteristic fragments in the range of m/z = 15–120. The high m/z range is dominated by C_{60}^{n+} ions (n = 1,2, inset). (B) Note the predominance of molecular ions at lower molecular weight and the increased abundance of the atomic species C^+ (m/z = 12) and C^{2+} (m/z = 6).

APT operational parameters, and spectral and spatial resolution for analyses on soft matter samples.

The Chiton tooth: a biomineral nanocomposite. Biological mineralized tissues—bone, tooth enamel, and mother-of-pearl—are sophisticated organic/inorganic composites. Optimized over hundreds of millions of years of evolution, organisms have achieved remarkable engineering feats, such as high bone toughness at low weight, self-sharpening teeth, and self-repair capability. In many biominerals, a preformed organic matrix interacts with the forming mineral and is occluded during mineralization. In bone, for example, hydroxylapatite nano-platelets are embedded in an organic matrix is that is made of collagen fibrils and some non-collagenous proteins. A back-of-the-envelope calculation shows that the surface area of the mineral is enormous, on the order of 1,000,000 m^2 in a human, which is a hundred times larger than the surface area of the capillaries of our blood vessels. Clearly, knowledge of the nano-scale architecture in biomineral nanocomposites is integral to our understanding of their function.

State-of-the-art electron tomography demonstrated that organic/inorganic interfaces can have very convoluted shapes in three dimensions, but the technique revealed little of the chemical complexity [19]. Even advanced electron microscopy using energy filtering or energy-loss spectroscopy is not well suited for detection and quantification of some of the low-Z elements (Na, Mg, K, organics) typical of biological materials. In contrast, APT has good sensitivity across the periodic table and offers sub-nanometer spatial resolution. This capability helped us detect a new level of chemical and structural hierarchy in the hardest biomineral known, the *Chaetopleura apiculata* (chiton) tooth cusp [17]. The teeth of the chiton (a kind of mollusk) are arranged in rows along the radula or rasping tongue (Figure 4A). The tooth is first synthesized as a free-standing organic scaffold comprised primarily of chitin fibers and a small amount of protein [20]. This scaffold is then mineralized as the tooth matures, occluding the organic fibers. Elemental maps of cross section of the tooth reveal the location of the hydroxyapatite [$Ca_5(PO_4)_3(OH)$] core and the magnetite [Fe_3O_4] cap (Figure 4B). The outstanding fracture toughness and wear resistance of the magnetite tooth cusp results from the organic/inorganic interfaces that deflect and arrest cracks [21].

We compared chiton tooth cusp samples containing both mineral and organics with geological magnetite as an inorganic reference compound and chitin thin-film samples as a reference for the organic material. All specimens where prepared for APT by FIB-liftout techniques and tip sharpening (Figure 5). The resulting TOF spectra (Figure 6) allowed us to clearly identify sets of peaks related to magnetite mineral, inorganic impurities, and organics. Reconstructions of chiton tooth mineral reveal organic fibers surrounded by magnetite (Figure 7). Remarkably, most fibers co-localize with either Na^+ or Mg^{2+}; and thus these elements have likely different functional roles in controlling fibre formation and matrix–mineral interactions. APT is uniquely able to detect this chemical/structural heterogeneity. We anticipate that laser-pulsed

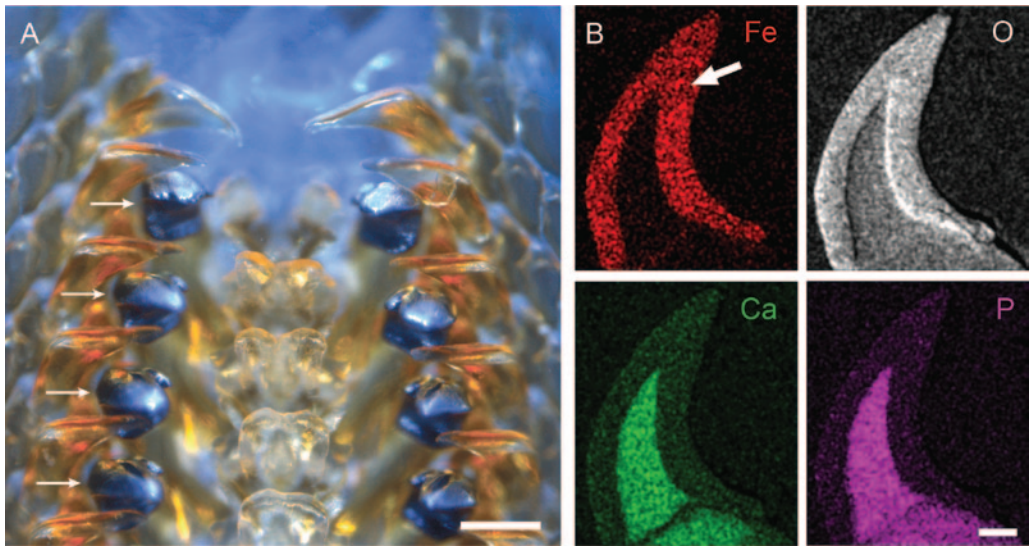

Figure 4: Chiton radula and tooth structure. (A) The tip of a *C. apiculata* radula, with 4 rows of teeth (arrows). Scalebar = 200 µm. (B) SEM-EDS elemental maps of tooth cross-section show apatite core and magnetite cap. Scalebar = 20 µm. Adapted from Ref. [17].

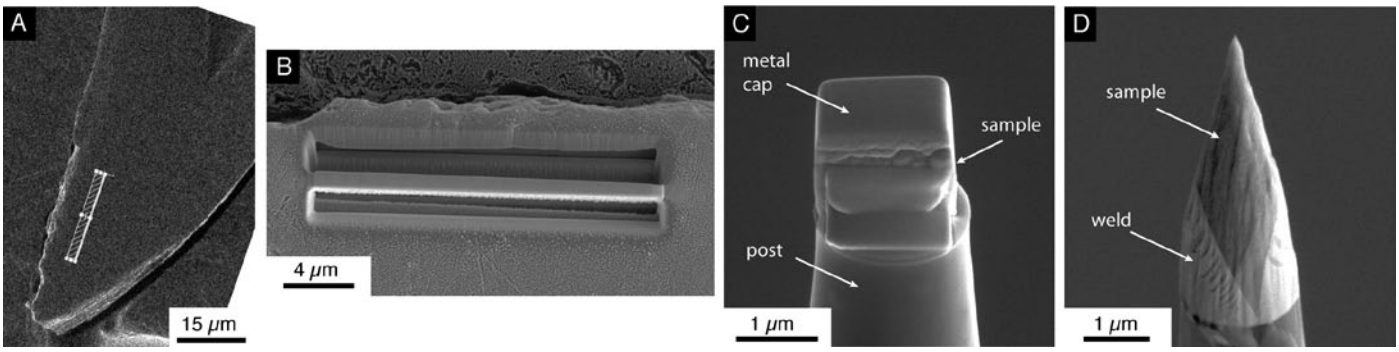

Figure 5: Preparation of chiton tooth samples for APT. (A) A protective metal strap is deposited *in situ* on a ground and polished section. (B) A sample wedge is created by FIB milling. The wedge is affixed to a micromanipulator, cut loose from the sample using FIB milling, and lifted out. (C) Pieces of the wedge are "welded" to a Si post array using *in situ*-deposited metal. (D) Annular FIB-milling results in a sharp sample tip.

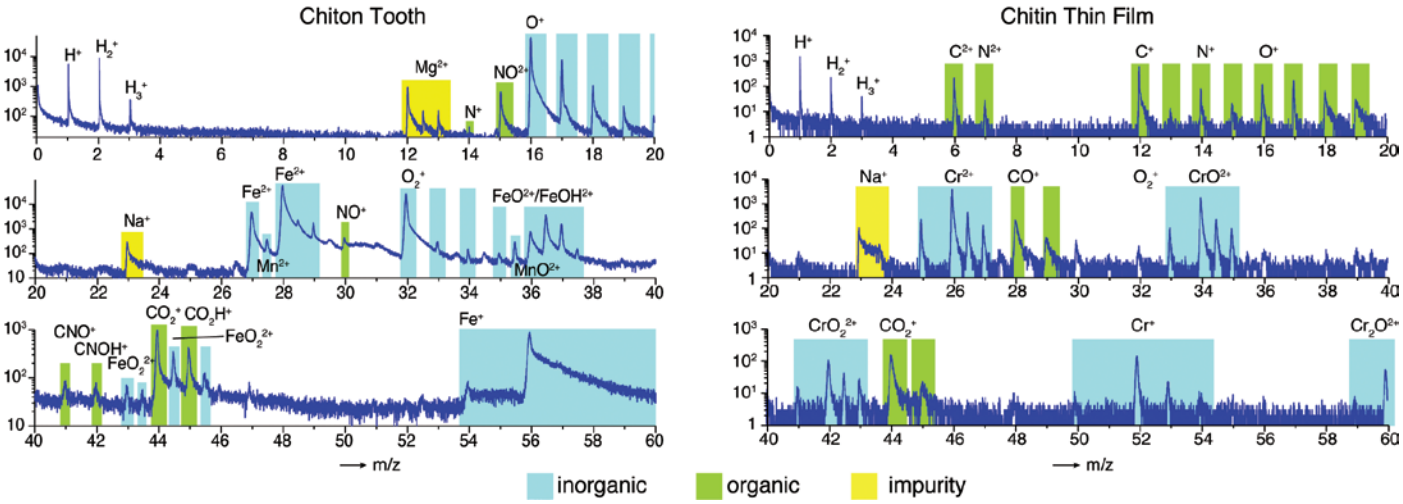

Figure 6: Atom probe time-of-flight spectra from the chiton tooth and a chitin thin film show the range of ions derived from the bulk inorganic (blue overlay), the organic matter (green overlay), and inorganic impurities (yellow overlay).

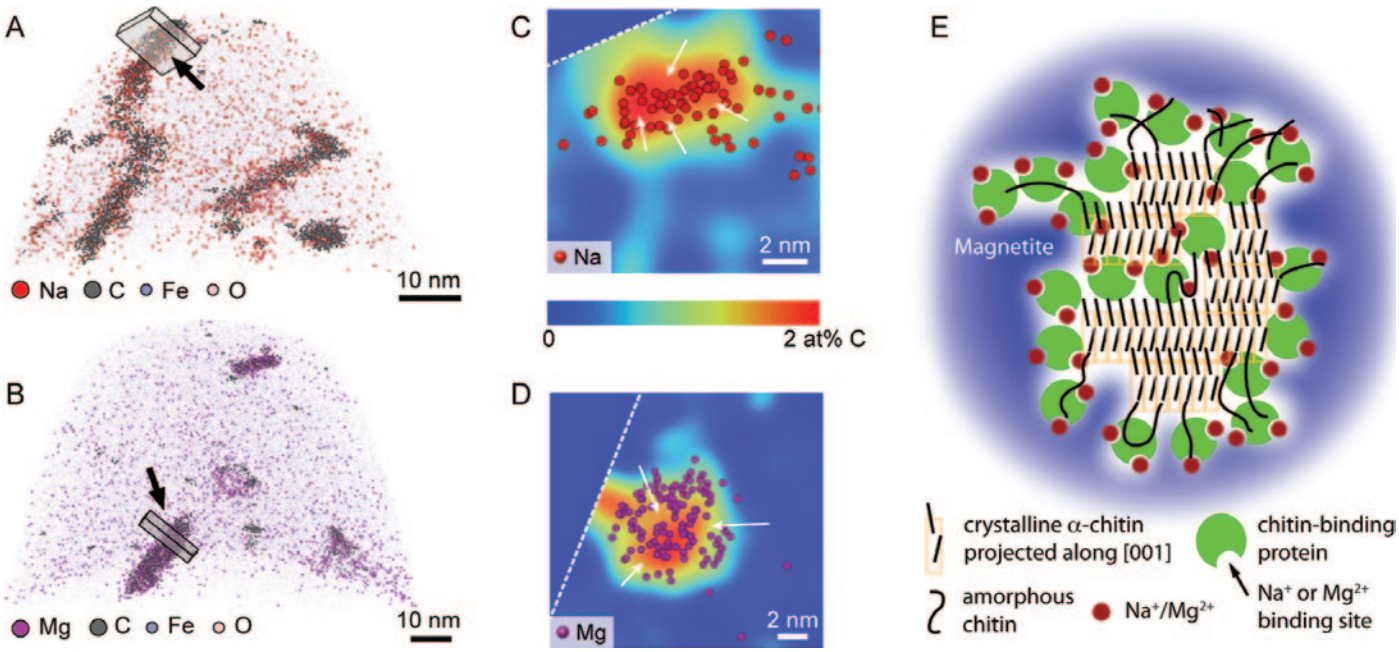

Figure 7: Three-dimensional reconstructions of the chiton tooth samples. (A) and (B) two representative samples from the chiton tooth with organic fibers that bind Na (A, red) or Mg (B, magenta), exclusively. (C) and (D) Overlay of Na^+ (C, red spheres) and Mg^{2+} (D, magenta spheres) positions on a 2-D carbon concentration map integrated over the boxed regions in A and D, respectively. (E) Proposed model for the architecture of the chiton tooth fibre. Adapted from Ref. [17].

APT will contribute greatly to our understanding not only of biomineral nanostructures, but also of synthetic organic/inorganic composites such as organic electronics, organic photovoltaic materials, and polymer nano-composites.

Conclusions

Laser-pulsed APT provides reconstructed images and mass spectra of organic materials and organic/inorganic interfaces. These data complement results from electron microscopy. Appropriate specimen preparation is essential in producing reliable images and spectra.

References

[1] P Verma, P Maire, and P Novak, *Electrochim Acta* 55 (2010) 6332–41.
[2] K Nomura, H Ohta, A Takagi, T Kamiya, M Hirano, and H Hosono, *Nature* 432 (2004) 488–92.
[3] MA Aronova, YC Kim, R Harmon, AA Sousa, G Zhang, and RD Leapman, *J Struct Biol* (2007) 160(1) 35–48.
[4] CJ Fahrni, *Curr Opin Chem Biol* 11 (2007) 121–27.
[5] R McRae, P Bagchi, S Sumalekshmy, and CJ Fahrni, *Chem Rev (Washington, DC, United States)* 109 (2009) 4780–4827.
[6] TF Kelly, O Nishikawa, JA Panitz, and TJ Prosa, *MRS Bull* 34 (2009) 744–50.
[7] O Nishikawa and H Kato, *J Chem Phys* 85 (1986) 6758–64.
[8] T Maruyama, Y Hasegawa, T Nishi, and T Sakurai, *J Phys* 48 (1987) 269–74.
[9] A Tolstogouzov, U Bardi, O Nishikawa, and M Taniguchi, *Int J Mass Spectrom* 281 (2009) 37–40.
[10] O Nishikawa, M Taniguchi, and A Ikai, *Appl Surf Sci* 256 (2009) 1210–13.
[11] Y Zhang and AC Hillier, *Anal Chem* 82 (2010) 6139–47.
[12] B Gault, WR Yang, KR Ratinac, RK Zheng, F Braet, and SP Ringer, *Langmuir* 26 (2010) 5291–94.
[13] A Stoffers, C Oberdorfer, and G Schmitz, *Langmuir* 28(1) (2012) 56–59.
[14] TJ Prosa, S Kostrna Keeney, and TF Kelly, *J Microsc* 237 (2010) 155–67.
[15] TJ Prosa, S Kostrna Keeney, and TF Kelly, *Microsc Microanal* 13 (2007) 190–91.
[16] TJ Prosa, SLP Kostrna, and TF Kelly, *50th International Field Emission Symposium* 2006, 533–34.
[17] L Gordon and D Joester, *Nature* 469 (2011) 194–97.
[18] MK Miller, KF Russell, K Thompson, R Alvis, and DJ Larson, *Microsc Microanal* 13 (2007) 428–36.
[19] H Li, HL Xin, ME Kunitake, EC Keene, DA Muller, and LA Estroff, *Advanced Functional Materials* 21 (2011) 2028–34.
[20] JA Shaw, PhD dissertation, Murdoch University (Perth), 2007.
[21] JC Weaver, Q Wang, A Miserez, A Tantuccio, R Stromberg, KN Bozhilov, P Maxwell, R Nay, ST Heier, E DiMasi, and D Kisailus, *Materials Today* 13 (2010) 42–52.

MT